ChemBioChem

Research Article
doi.org/10.1002/cbic.202200202

Chemistry Europe
European Chemical Societies Publishing

www.chembiochem.org

Histidine Ligated Iron-Sulfur Peptides

Luca Valer,[a, b] Daniele Rossetto,[a, b] Taylor Parkkila,[b] Lorenzo Sebastianelli,[b] Graziano Guella,[c] Amber L. Hendricks,[d] James A. Cowan,[d] Lingzi Sang,[b] and Sheref S. Mansy*[a, b]

Iron-sulfur clusters are thought to be ancient cofactors that could have played a role in early protometabolic systems. Thus far, redox active, prebiotically plausible iron-sulfur clusters have always contained cysteine ligands to the cluster. However, extant iron-sulfur proteins can be found to exploit other modes of binding, including ligation by histidine residues, as seen with [2Fe-2S] Rieske and MitoNEET proteins. Here, we investigated the ability of cysteine- and histidine-containing peptides to coordinate a mononuclear Fe^{2+} center and a [2Fe-2S] cluster and compare their properties with purified iron-sulfur proteins. The iron-sulfur peptides were characterized by UV-vis, circular dichroism, and paramagnetic NMR spectroscopies and cyclic voltammetry. Small ($\leq$6 amino acids) peptides can coordinate [2Fe-2S] clusters through a combination of cysteine and histidine residues with similar reduction potentials as their corresponding proteins. Such complexes may have been important for early cell-like systems.

Introduction

Although iron-sulfur clusters are primarily coordinated by four cysteinyl ligands,[1] there are several cases where the cluster is not completely ligated by cysteines. For example, mononuclear, [2Fe-2S], and [4Fe-4S] clusters can be ligated by the sidechain of an Asp, Glu, or His.[2] Of these, ligation by His is rarer. Two examples of His ligated iron-sulfur clusters are found in Rieske and MitoNEET, which coordinate a [2Fe-2S] cluster with two Cys and two His, and with three Cys and one His, respectively. One notable effect of ligation by His is a shift in reduction potential of the cluster. [2Fe-2S] clusters solely coordinated by Cys, as found in ferredoxins, display reduction potentials from −150 to −400 mV (vs SHE),[3] while His coordination shifts the reduction potential to more positive values. The [2Fe-2S] clusters of MitoNEET have potentials from −100 mV to +50 mV.[4] The reduction potentials of [2Fe-2S] Rieske clusters vary from −150 to +400 mV.[5] The protonation state of the coordinated His impacts the reduction potential of the iron-sulfur cluster, and so alterations of the pK_a of the His can be used to fine-tune potentials.[6] Such a strategy was used to adjust the reduction potential of MitoNEET across a 700 mV range.[7]

The synthesis of non-proteinaceous iron-sulfur clusters has a long history. Holm and colleagues expertly deciphered the rules governing the assembly of all the major types of iron-sulfur clusters found in biology.[8] Although these reactions were typically in organic solvent, their characteristics were similar to their protein bound counterparts in aqueous solution. More recently, iron-sulfur clusters coordinated by small peptides in aqueous solution have been investigated.[9] The most well characterized of these are the ferredoxin maquettes from the Dutton group, where 15–20 amino acid peptides, based on natural protein sequences, were synthesized and found to coordinate a $[4Fe\text{-}4S]^{2+/+}$ cluster.[10] More recent efforts have focused on the synthesis of model prebiotic iron-sulfur peptides.[11] However, none of these previous efforts have demonstrated the ligation of an iron-sulfur cluster by imidazole or an imidazole sidechain with a non-protein scaffold in water. To determine if such clusters could be built in aqueous solution, we synthesized peptides between 5 and 25 amino acids in length containing Cys and His residues and compared their ability to coordinate iron-sulfur clusters with recombinant iron-sulfur proteins. Human ferredoxin and the soluble respiratory-Type Rieske protein from *Thermus thermophilus* were chosen as examples of [2Fe-2S] clusters.[12] *Clostridium pasteurianum* rubredoxin was the representative of a mononuclear center. Mutants of each were generated for comparison to the synthesized peptides. Mononuclear Fe^{2+}-peptides were spectroscopically different from rubredoxin but possessed similar reduction potentials. While the data were inconclusive for His ligation of mononuclear centers, UV-Visible absorption and NMR spectra in addition to reduction potentials were consistent with the ligation of [2Fe-2S] clusters by His-containing peptides.

[a] L. Valer, D. Rossetto, S. S. Mansy
D-CIBIO, University of Trento
via Sommarive 9, 38123 Trento 28123 (Italy)
[b] L. Valer, D. Rossetto, T. Parkkila, L. Sebastianelli, L. Sang, S. S. Mansy
Department of Chemistry, University of Alberta
11227 Saskatchewan Drive
Edmonton T6G 2G2, Alberta (Canada)
E-mail: sheref.mansy@ualberta.ca
[c] G. Guella
Department of Physics, University of Trento
Via Sommarive 14, Trento 38123 (Italy)
[d] A. L. Hendricks, J. A. Cowan
Department of Chemistry and Biochemistry
The Ohio State University
100 West 18th Ave, Columbus, OH 43210 (USA)

Supporting information for this article is available on the WWW under https://doi.org/10.1002/cbic.202200202

© 2022 The Authors. ChemBioChem published by Wiley-VCH GmbH. This is an open access article under the terms of the Creative Commons Attribution Non-Commercial License, which permits use, distribution and reproduction in any medium, provided the original work is properly cited and is not used for commercial purposes.

© 2022 The Authors. ChemBioChem published by Wiley-VCH GmbH

Results and Discussion

Reference Iron-sulfur proteins

Recombinantly expressed and purified Rieske proteins were prepared to generate reference UV-Vis absorption spectra. Their spectra were consistent with past reports,[12–14] with peaks at 450 nm and 580 nm (Figure 1C). Mutant constructs (Table 1) in which one of the His or both of the His were substituted with Cys possessed UV-vis spectra similar to MitoNEET and ferredoxin, respectively. H90 C Rieske (1 His, 3 Cys ligands) had a prominent peak at 470 nm (Figure 1D), and H90 C H107 C Rieske (4 Cys ligands) displayed absorption maxima at 420 nm and 450 nm (Figure 1E). Since Rieske proteins contain a disulfide bond between C93 and C109, it was possible that the recombinantly expressed constructs in which ligating His were substituted led to the recruitment of C93 and/or C109 for the stabilization of the cluster. To confirm that the [2Fe-2S] cluster was coordinated by the original positions of the ligands, the Cys involved in the formation of the disulfide bond were substituted with Ala. C93A H107C C109 A and H90C C93A H107C C109A Rieske showed absorption and visible CD spectra similar to constructs that contained C93 and C109 (Figures S1–S2). Continued coordination of the [2Fe-2S] cluster in the absence of a disulfide bond was consistent with past reports.[15] Recombinantly expressed rubredoxin had absorption maxima at 380 nm, 490 nm, and a shoulder at 580 nm (Figure 1A).

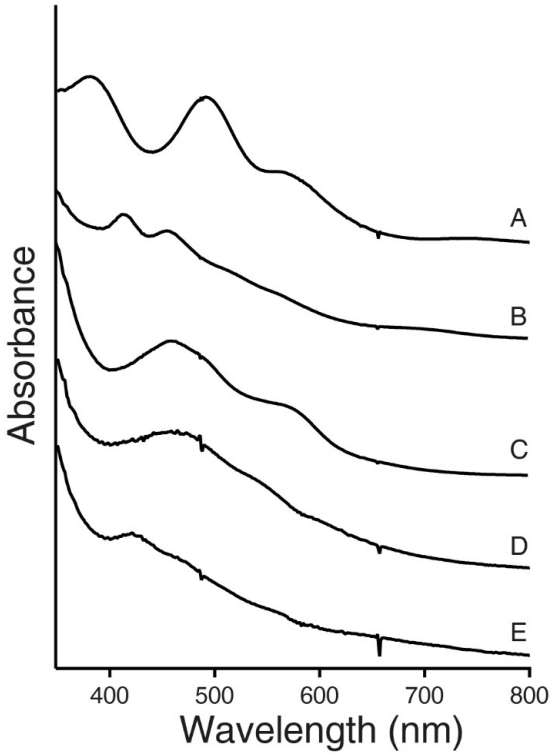

Figure 1. UV-vis spectra of oxidized iron-sulfur proteins. A. Wild Type (WT) rubredoxin (4 Cys ligands). B. WT human ferredoxin (4 Cys ligands). C. WT Rieske (2 His, 2 Cys ligands). D. H90C Rieske (1 His, 3 Cys ligands). E. H90C H107C Rieske (4 Cys ligands).

Table 1. Iron-sulfur proteins and peptides used in this study.

Name[a]	Protein/peptide sequence[b]
WT Rieske ROI	VCTHLGCIVSQWVADEEAALCPCHG
H90C Rieske ROI	VCTCLGCIVSQWVADEEAALCPCHG
H90C H107C ROI	VCTCLGCIVSQWVADEEAALCPCCG
C93A C109A ROI	VCTHLGAIVSQWVADEEAALCPAHG
H90C C93A C109A ROI	VCTCLGAIVSQWVADEEAALCPAHG
H90C C93A H107C C109A ROI	VCTCLGAIVSQWVADEEAALCPACG
CXH peptide	GCTHG
CXC peptide	GCTCG
CXXH peptide	GCPAHG
CHCH linear	VCTHLGAIVSQWVADEEAALCPAHG
CCCH linear	VCTCLGAIVSQWVADEEAALCPAHG
CCCC linear	VCTCLGAIVSQWVADEEAALCPACG
CHCH stapled	VCTHLGDIVSLCPKHG
CCCH stapled	VCTCLGDIVSLCPKHG
CCCC stapled	VCTCLGDIVSLCPKCG
WT Rubredoxin ROI	TCTVCG...VCPLCG
C42H Rubredoxin ROI	TCTVCG...VCPLHG
C9H C42H ROI	TCTVHG...VCPLHG
CXXC peptide	GCTVCG
CXXH peptide	GCTVHG
CXXC peptide	GCPLCG
CXXH peptide	GCPLHG
WT Ferredoxin ROI	ACEGTLACSTCH...GCQ

[a] ROI indicates the region of interest of the protein. [b] Positions in bold indicate coordinating residues. Underlined residues indicate the position of the original disulfide bond, which was substituted with a lactam bridge for the stapled peptides. The "…" of rubredoxin indicates 27 amino acids and 34 amino acids for ferredoxin.

However, the spectra of both C42H rubredoxin and C9H C42H rubredoxin were greatly diminished in intensity (Figure S3).

To investigate the ability of small peptides containing both Cys and His to coordinate metal ions similarly to proteins, fourteen different peptides and N-acetyl Cys methyl ester (N–Ac-Cys-OMe) and N-acetyl His methyl ester (N–Ac-His-OMe) were incubated with Fe^{2+}, Co^{2+}, and Zn^{2+} and spectroscopically evaluated. Cys-containing peptides, but not peptides that contained both Cys and His, were previously demonstrated to coordinate transition metals.[16,17] Here, we focused on the binding of Fe^{2+} because iron ions were easily accessible before

© 2022 The Authors. ChemBioChem published by Wiley-VCH GmbH

the great oxidation event,[18] are frequently found in model prebiotic pathways,[19–22] and are exploited throughout extant metabolism. Zn^{2+} was investigated because this metal ion can bind to the same motifs as iron-sulfur clusters,[2] and Zn^{2+} has been hypothesized to be important in early evolution.[23] Co^{2+} is a useful probe that facilitates studies with the spectroscopically silent Zn^{2+} through metal substitution.[24] The majority of the exploited peptide sequences were derived directly from sequences found in iron-sulfur proteins (Table 1). For example, the four ligands to the [2Fe-2S] cluster of Rieske are within a 25 amino acid region of the protein that contains CXH and CXXH motifs. Two CXC/H-containing pentapeptides (GCTHG and GCTCG) and one CXXH-containing hexapeptide (GCPAHG) were tested. Three 25 amino acid peptides that encompassed the entire [2Fe-2S] binding site of the Rieske protein from *T. thermophilus* were also synthesized with the Cys disulfide positions substituted with Ala. Longer peptides with four Cys were previously found to stabilize the formation of [2Fe-2S] clusters.[25] These 25 amino acid peptides either contained two (CHCH), three (CCCH), or four (CCCC) Cys residues (Scheme S1). Finally, three smaller (16 residues), stapled versions of the peptide with four potential ligands to the cluster were synthesized (Scheme S2). Staples were used to attempt to spatially organize the ligands for the binding of cluster. Stapled versions of the 25-residue peptide failed, likely due to the distance and flexibility within the peptide between the side-chains that would form the staple.[26] The smaller 16-residue version was designed by removing the residues involved in the formation of an intervening anti-parallel β-sheet[27] in between the CXH and CXXH motifs. The staple was a lactam bridge formed by using an orthogonal protecting group strategy during synthesis, which led to the covalent joining of the side chains of Asp and Lys. Rubredoxin contains two CXXC motifs separated by 27 amino acids. Four hexapeptides based on these motifs were synthesized, including GCTVCG, GCTVHG, GCPLCG, GCPLHG (Table 1). A GCG peptide was prepared and served, along with N–Ac-Cys-OMe and N–Ac-His-OMe, as a representative molecule containing a single potential ligand to the metal center.

Absorption spectra of mononuclear Co^{2+} and Fe^{2+} centers

Metal binding was first evaluated with Co^{2+}, as the UV-visible absorption spectra of Co^{2+} complexes are easily interpretable in terms of the number of Cys ligands.[24] All of the small peptides (≤ six residues) with two Cys and no His showed an absorbance peak at 750 nm, consistent with coordination by four thiolates (Figure 2A).[24] To achieve such coordination, two peptides would have had to bind a single Co^{2+}. When one of the Cys was substituted with a His, the absorbance peak shifted to 660 nm, as would be expected for a complex with two Cys and two His ligands (Figure 2B).[24] The longer linear and stapled Rieske peptides with four potential ligands to the metal ion gave UV-vis spectra congruent with the number of Cys residues. CHCH, CCCH, and CCCC Rieske peptides had absorbance maxima at

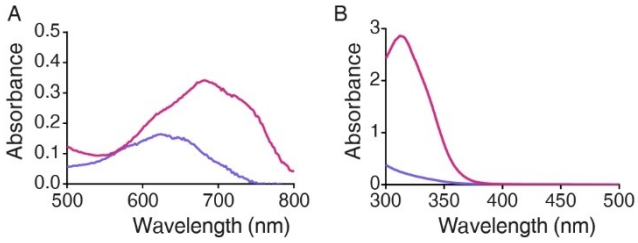

Figure 2. Comparison between all Cys and mixed Cys - His coordination for Co^{2+} and Fe^{2+}. UV-vis spectra of Co^{2+} (A) and Fe^{2+} (B) coordinated to GCTVCG (red) and GCTVHG (blue). Conditions were 1.25 mM peptide, 1 mM metal ion, 20 mM Gly-Gly, pH 8.8.

660 nm, 710 nm, and 750 nm, respectively, when bound to Co^{2+} (Figure S4).

The UV-vis spectra of peptidyl complexes with Fe^{2+} were less clearly interpretable than spectra with Co^{2+} and were unlike that of rubredoxin. Absorption spectra with Fe^{2+} either showed a clear peak at 315 nm when coordination by four Cys was possible or a shoulder in the 300–310 nm when His was present (Figures 2B-S5-S6-S7). The only exceptions were N–Ac-Cys-OMe, which gave a featureless UV-vis spectrum above 250 nm, and N–Ac-His-OMe, which showed a broad shoulder below 300 nm (Figure S8). To confirm the coordination of Fe^{2+}, paramagnetic ^{1}H NMR spectra were acquired. The paramagnetism of the Fe^{2+} center gives rise to hyperfine shifted resonances of Cys Hα in the 10–20 ppm region and Cys Hβ within the 100–300 ppm range.[28] The paramagnetic ^{1}H NMR spectra of the Cys-containing peptides incubated with Fe^{2+} showed the presence of such paramagnetically shifted resonances of Cys Hα and Cys Hβ (Figure S9A-9B). Paramagnetically shifted resonances were not detected for peptides containing His (Figure S10A). The addition of Fe^{2+} to the 25 residue Rieske-like peptides and the shorter Stapled peptides led to broad, featureless absorption in the UV-Vis region, with absorption increasing with increasing number of Cys (Figure S11). The stapled peptide absorbed more strongly than the 25 residue peptides upon the addition of Fe^{2+}.

Peptide affinities for Co^{2+}, Zn^{2+}, and Fe^{2+}

We next evaluated the binding affinity for Co^{2+}, Zn^{2+}, and Fe^{2+}. Since Zn^{2+} complexes do not absorb in the UV-Vis region, the affinity for Zn^{2+} was determined by substitution of bound Co^{2+}. Binding affinities for N–Ac-Cys-OMe, N–Ac-His-OMe, and GCG i.e. molecules with only one potential ligand, were always less than peptides that contained more than one potential ligand for all three metal ions. Molecules with two ligands possessed, on average, 2.7-fold greater affinity for the tested metal ions, and peptides with four potential ligands bound the metal ions 2.8-fold more tightly than peptides with two ligands (Figures S12–S13–S14). Affinities followed the Irving-Williams series, with peptides binding Zn^{2+} more strongly than Co^{2+} followed by Fe^{2+}. There was a stronger sequence dependence, confirmed by calculations of coefficients of variation, of affinities for Fe^{2+}

© 2022 The Authors. ChemBioChem published by Wiley-VCH GmbH

followed by Zn^{2+} and then Co^{2+} (Figure 3 and Tables S1–S2). For Fe^{2+}, the preference for Cys ligands over His ligands was most evident for the two ligand containing peptides (Figure 3, blue bars). Of these, peptides that contained two Cys residues bound Fe^{2+}, on average, 5.9-fold greater than peptides with one Cys and one His. The Linear Rieske (CCCC) peptide bound all the tested metal ions more strongly than the other Linear Rieske peptides (Figures S15–S16–S17). Conversely, of the Stapled Rieske peptides, the best binder was (CHCH), i.e. the peptide that contained two Cys and two His ligands. The lactam bridge may have helped pre-organize the Cys and His for binding and thus decreased the entropic cost associated with coordination.

Absorption spectra of [2Fe-2S] peptides

To determine whether the synthesized peptides could coordinate a [2Fe-2S] cluster, each peptide was anaerobically incubated with Fe^{3+} and HS^-. The ratio of ligating residues (L) to Fe^{3+} and HS^- (i.e. L:Fe^{3+}:HS^-) was 16:1:1. The UV-vis spectra of Cys containing small ($\leq$ 6 amino acids) peptides that lacked His residues showed bands at 420 nm and 450 nm indicative of a ferredoxin-like [2Fe-2S] cluster (Figure 4A and S18A-S19 A).[29] Near-UV-visible circular dichroism (CD) spectra showed a band at 470 nm that was similar to the 450 nm peak seen with ferredoxin, but with lower molar ellipticity (Figure S20A). Paramagnetic ^{1}H NMR spectra confirmed the presence of the $[2Fe\text{-}2S]^{2+}$ cluster with a broad resonance at 30 ppm (Figure S9D).[28] The NMR spectrum also revealed the continued presence of the mononuclear center that was not observable by UV-vis absorption (Figure S9C). Such a result was not surprising, since peptides exist in an equilibrium between the coordination of a mononuclear center and a [2Fe-2S] cluster when in an environment containing iron and sulfide ions.[28] Conversely, UV-Vis absorption spectra of small ($\leq$ 6 amino acids) peptides that possessed both Cys and His residues did not resemble the spectra of ferredoxin or the Rieske protein (Figure 4B-S18BC–S19B). Although there was absorption in the visible region, no clear peaks were discernable, and their CD spectra were featureless (Figure S14B). Paramagnetic ^{1}H NMR spectra showed sharp peaks near 10 ppm and 30 ppm in addition to a shoulder at 13 ppm (Figure S7B). The peak at 30 ppm was consistent with previously reported spectra of Rieske proteins;[5,30] however, the data were not sufficient to distinguish between four peptides, each providing a single Cys to a single cluster or two peptides that ligated the [2Fe-2S] with two Cys and two His in total. In the presence of Fe^{3+} and HS^-, UV-Vis spectra were indicative of the presence of a ferredoxin-like $[2Fe\text{-}2S]^{2+}$ cluster for Linear peptides CCCH and CCCC and not for the more Rieske-like sequence found in the Linear CHCH peptide (Figure S21A-S21C–S21E). UV-Vis spectra of the stapled peptide lacked well defined peaks, but as seen with the Linear peptides, the bands became more prominent as the number of Cys increased (Figure S21B-S21D–S21F). The data suggested that the Linear peptides better stabilized the formation of a $[2Fe\text{-}2S]^{3+}$ cluster than the Stapled peptides (Figures S22–S23–S24–S25–S26–S27).

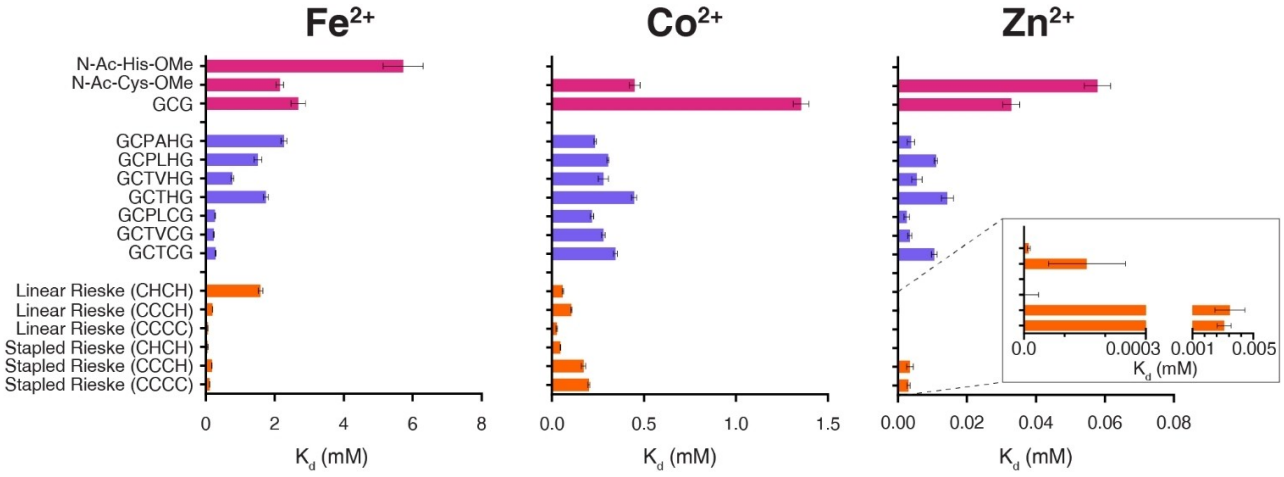

Figure 3. K_d of peptides for Fe^{2+}, Co^{2+}, and Zn^{2+}. Data obtained represent mean and SD of distinct samples, n = 3. Peptides with a single ligand (Cys or His) are in red, peptides with two ligands are in blue, and peptides with four ligands are in orange. The K_d of N–Ac-His-OMe is not reported for Co^{2+} and Zn^{2+}.

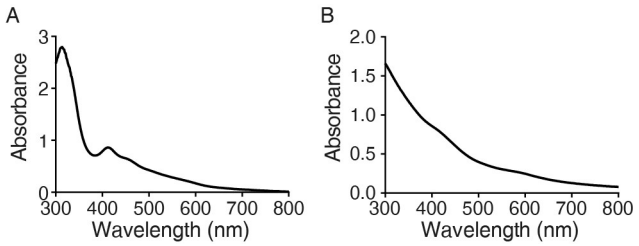

Figure 4. UV-vis spectra $[2Fe\text{-}2S]^{2+}$ cluster coordinated by small peptides. A. $[2Fe\text{-}2S]^{2+}$ coordinated by GCTVCG. B. $[2Fe\text{-}2S]^{2+}$ coordinated by GCTVHG. Solution conditions were 4 mM peptide, 0.5 mM $FeCl_3$, 0.5 mM Na_2S, pH 8.8.

© 2022 The Authors. ChemBioChem published by Wiley-VCH GmbH

Cyclic voltammetry confirms His-coordination to [2Fe-2S] clusters

Reduction potentials of iron-sulfur clusters are strongly influenced by their ligands. The substitution of a negatively charged Cys ligand with a neutral His typically increases the reduction potential of the cluster. Therefore, to confirm whether the His residues were ligating the iron ions, cyclic voltammetry was carried-out on the prepared complexes. All of the mononuclear complexes had reduction potentials in the range expected for rubredoxin-like proteins,[31] and other reported mononuclear centers coordinated by small thiol-containing molecules (Figures S28–S29–S30–S31–S32–S33–S34–S35–S36, Table S3).[22] The most negative reduction potential measured was for N–Ac-Cys-OMe (−104±21 mV; all reduction potentials are vs. SHE). The most positive reduction potential was that of the pentapeptide GCTHG (+16±1 mV) (Figure 5A). Complexes of Fe^{2+} with N–Ac-Cys-OMe and GCG had lower reduction potentials than peptides containing two potential ligands to the iron ion. Although the average reduction potentials were greater for His-containing peptides, the values were within error. Therefore, it was not possible to confirm ligation by His for the mononuclear complexes.

Conversely, cyclic voltammetry of [2Fe-2S] clusters coordinated to peptides showed two different types of behavior (Figures S37-S38-S39-S40-S41-S42-S43-S44, Table S4). The all Cys containing peptides had reduction potentials in the range of −210 mV to −231 mV, with the exception of GCG (−117±12 mV). The data were similar to [2Fe-2S] ferredoxin with four ligating Cys. The peptides that contained both His and Cys gave more positive reduction potentials between −63 mV and −83 mV (Figure 5B), as would be expected for ligation by His, and similar to Rieske proteins.[4] We were not able to determine the reduction potentials of all the peptides, because several did not produce distinguishable reduction and oxidation peaks. These peptides included GCPLCG, GCTCG, and most of the Linear and Stapled Riske peptides. The only exceptions were the Stapled Rieske peptides with two Cys and two His (CHCH) and with three Cys and 1 His (CCCH), which had reduction potentials of −63 mV and −49 mV, respectively, consistent with coordination by His.

The reduction potential of Rieske proteins is pH dependent.[32] Lower pH leads to increased protonation of the ligating His and thus higher reduction potential. Therefore, if the investigated peptides bound the iron-sulfur cluster, in part, through His residues, then the reduction potential would be expected to be influenced by pH. Two [2Fe-2S] peptides, one lacking His (GCTVCG) and one containing His (GCTVHG) were subjected to cyclic voltammetry between pH 7.8 and 9.8. As expected, the reduction potential of the [2Fe-2S] cluster coordinated by GCTVHG decreased as the pH increased with a 92 mV/pH dependence (Figure 6C). Rieske proteins show a similar dependence (120 mV/pH).[33] Conversely, the reduction potential of the [2Fe-2S] cluster coordinated to GCTVCG was consistently near −230 mV between pH 8.3 and 9.8 (Table S4). Data are not reported at pH 7.8, because [2Fe-2S] GCTVCG was not stable at this pH. The data were consistent with the His residues coordinating the iron-sulfur cluster.

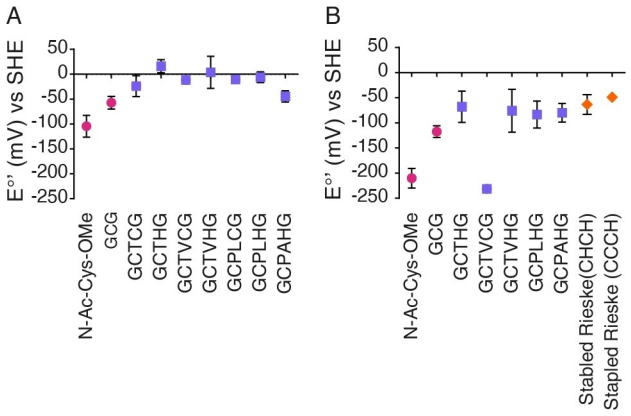

Figure 5. Measured formal reduction potentials of iron-sulfur peptides. A. Measured potentials of mononuclear centers stabilized by small peptides (vs. SHE). B. Measured potential of [2Fe-2S] peptides. Data obtained represent mean and SD of distinct samples, n=3 replicates. Conditions were 16 mM ligating residues, 1 mM $FeCl_3$, 1 mM Na_2S, pH 8.8. Red circle, 1 ligand; blue square, 2 ligands; orange diamond, Stapled CHCH and CCCH peptides.

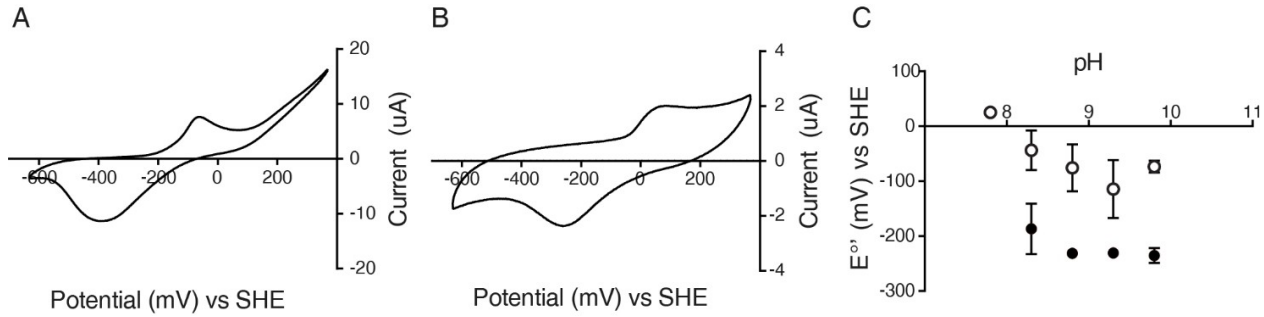

Figure 6. Cyclic voltammetry of [2Fe-2S] peptides. Cyclic voltammetry of [2Fe-2S] GCTVCG (A) and [2Fe-2S] GCTVHG (B). Conditions were 16 mM peptide, 2 mM $FeCl_3$, 2 mM Na_2S, pH 8.8, scan rate 100 mV/s. C. Formal reduction potentials of [2Fe-2S] GCTVCG (filled circles) and [2Fe-2S] GCTVHG (open circles) at different pH. Measurements were on 8 mM peptide, 1 mM $FeCl_3$, 1 mM Na_2S, pH 8.8 with a scan rate of 100 mV/s. At pH 7.8 the cluster coordinated by GCTVCG was not formed. Data obtained represent mean and SD of distinct samples, n=3 replicates.

© 2022 The Authors. ChemBioChem published by Wiley-VCH GmbH

Conclusions

Due to their central role in metabolism and the ease with which these metallocofactors form, there has been much speculation as to how iron-sulfur clusters could have impacted the origins of life.[34] Thus far, peptidyl mimics of prebiotic iron-sulfur clusters have focused on thiolate coordination; however, extant electron transfer pathways additionally make use of Fe^{2+} coordinated to His and porphyrins with steps mediated by organic molecules and other metal ions.[35] Although His is often argued to be prebiotically implausible because of phylogenetic analyses, phylogeny tells us little about the breadth of chemistry that transpired on the prebiotic Earth.[36] Nevertheless, the prebiotic presence of His remains unclear. Oro and coworkers did show that His can be synthesized from erythrose and formamidine.[37,38] However, the reaction is inefficient and relies on high concentrations of formamidine, which rapidly hydrolyzes.[39] Similar ambiguities existed for Cys in the past. Cys was frequently referred to as prebiotically implausible, and an analysis of the 1958 H_2S-rich spark discharge experiment showed the presence of the break-down products of Cys rather than Cys itself.[40,41] However, more recent efforts have uncovered prebiotically plausible routes to Cys.[42] Our data do not speak to the prebiotic plausibility of peptides that contain these amino acid residues but rather to their characteristics.

To determine if simpler analogues of the electron transport chain could have predated the complex pathways observed today, data are needed regarding the formation of different metallocomplexes and their electron transfer characteristics. Contemporary proteins can tune the reduction potential of their metallocofactor through subtle interactions arising from the local environment created within a complex tertiary fold. Here, we show that in the absence of such evolved scaffolds, [2Fe-2S] clusters can form coordinated to peptides containing Cys and His ligands with reduction potentials distinct from iron-sulfur peptides that rely on complete cysteinyl coordination. Since ligation by His shifts the reduction potential by 150 mV, iron-sulfur peptide-dependent electron transport chains much simpler than found in biology today may have been possible.

Experimental Section

Protein expression and purification: Plasmids encoding rubredoxin and Rieske iron-sulfur proteins and their respective mutants were synthesized by Genscript and inserted into pMal-c4x (NEB), generating a Maltose Binding Protein (MBP) tag. The plasmid encoding ferredoxin was synthesized by Genscript and inserted in pET-21b. Human ferredoxin was not tagged. Recombinant expression of the genes in pMal-c4x was with *Escherichia coli* NEBExpress. Recombinant expression of ferredoxin was with *E. coli* BL21(DE3) pLysS. For both, transformed cells were grown overnight at 37 °C in 10 mL Luria-Bertani (LB) supplemented with ampicillin (50 mg/mL). 1 mL of this starter culture was used to inoculate 1 L LB with 50 mg/mL ampicillin in a 5 L flask and grown at 37 °C with shaking to an OD^{600} of 0.6. Expression was induced with 0.4 mM of isopropyl β-D-1-thiogalactopyranoside (IPTG) and incubated at room temperature for an additional 15 h. Cells were harvested by centrifugation at 4000 x g for 15 min. The cell pellet was resuspended in 40 mL of sonication buffer (20 mM Tris HCl, 200 mM NaCl, pH 7.6,) and lysed by sonication (20 cycles of 10 s pulses followed by 50 s incubation on ice). Cellular debris was removed by centrifugation at 15000 x g for 15 min. For the purification of the MBP-tagged proteins, the lysate was loaded on an amylose column (NEB) and washed with 20 column volumes of amylose column buffer (20 mM Tris HCl, 200 mM NaCl, 0.1 mM EDTA, pH 7.6). The protein was eluted with 10 mM maltose in column buffer. The colored fractions were collected and concentrated using Amicon Ultra centrifugal filter units (MWCO 10 kDa). Proteins were dialyzed against 20 mM Tris HCl, pH 7.6 overnight at 4 °C. Ferredoxin was purified in two-steps, as previously reported.[29] The first step of the purification exploited an ion exchange column with DEAE resin (Bio-Rad) and washed with 20 column volumes of DEAE column buffer (50 mM Tris-HCl, pH 7.4). The proteins were eluted with a 90 mL gradient of 0–500 mM NaCl in DEAE column buffer. The protein eluted at approximately 350–400 mM NaCl. The colored fractions were collected and concentrated with Amicon Ultra centrifugal filter units (MWCO 10 kDa). The second step of the purification relied on size-exclusion chromatography with a HiLoad 16/600 Superdex 75 pg column and a FPLC (Äkta pure, GE Healthcare). Subsequently, the protein-containing fractions were collected and concentrated with Amicon Ultra centrifugal filter units (MWCO 10 kDa).

Peptide synthesis: Peptides were synthesized via solid phase peptide synthesis, as previously described.[11] *N*,*N*-Dimethyl formamide (DMF) was used as the solvent and Wang resin (Fmoc-Gly-Wang) was used as the starting polymeric support. Trityl-protected Fmoc-cysteine (Fmoc-Cys(Trt)-OH) and *tert*-butyl (OtBu) side chain-protected Fmoc-α-amino acids were used as the building blocks. The peptide chain was elongated by sequential Fmoc deprotection of the residue anchored to the resin and Fmoc-AA-OH coupling. Fmoc deprotection was obtained by washing the mixture with 20% (v/v) solution of piperidine in DMF. For each coupling, an excess (Fmoc-AA-OH: anchored AA, 4:1) of the Fmoc-α-amino acid derivative was added to the resin. Apart from Fmoc-Cys(Trt)-OH, Fmoc-α-amino acid derivatives were activated with a mixture of hydroxyl-benzotriazole (HOBt), *N*,*N*,*N*′,*N*′-tetramethyl-O- (benzotriazol-1-yl)uronium tetrafluoborate (TBTU), and *N*,*N*-diisopropylethyl amine (DIPEA). Fmoc-Cys(Trt)OH was activated with a *N*,*N*′-diisopropylcarbodiimide (DIC)/HOBt mixture. For the cyclized peptides, Fmoc protected Asp (Allyl) and Lys (Alloc) were used. After the synthesis of the full peptide, before the last Fmoc deprotection, Asp and the Lys were deprotected by treatment with 0.5 equiv. $Pd(PPh_3)_4$, 10 equiv. of $PhSiH_3$ for 2 h, in the dark under constant flux of N_2 and repeated twice. After deprotection, the resin was washed five times with dichloromethane (DCM), sodium diethyldithiocarbamate in DMF (0.1% w/w) and DMF. Cyclization was achieved with a 24 h treatment hydroxyl-benzotriazole (HOBt), *N*,*N*-diisopropylethyl amine (DIPEA), and (7-azabenzotriazol-1-yloxy)tripyrrolidinophosphonium hexafluorophosphate (PyAOP) in DMF. At the end of the synthesis, the polymers were cleaved from the resin and deprotected by treatment with a solution of trifluoroacetic acid (TFA):H_2O:triisopropyl silane (TIS):1,2-ethanedithiol (EDT) (97:1:1:1, v/v) for 2 h. The product was precipitated with cold diethyl ether/petroleum ether (30:70, v/v) followed by washing cycles with diethyl ether. The peptides were finally solubilized in 20% acetic acid (v/v), flash frozen in liquid nitrogen, and lyophilized overnight at −84 °C (Labconco FreeZone Freeze Dryer). The stapled peptides were further purified by HPLC (Agilent 1100 Series) with a reverse phase Zorbax SB–C12 column (Agilent Technologies) using H_2O and acetonitrile (both containing 0.1% TFA) as the mobile phase. The gradient was from 20% to 100% acetonitrile over 15 min. After purification, fractions containing peptide were lyophilized overnight at −84 °C.

Synthesis of the clusters: All steps were carried-out under anoxic conditions inside a Genesis 2P glovebox system (Vacuum Atmos-

© 2022 The Authors. ChemBioChem published by Wiley-VCH GmbH

pheres Company) with $O_2 < 1$ ppm. The peptides were dissolved in ultrapure degassed H_2O (Synergy UV water purification system, Merck, Darmstadt, Germany) and the pH was adjusted to pH 8.8 using NaOH (5 M), if not specified otherwise. For the formation of the mononuclear complex, $FeCl_3$ was added from a 0.33 M stock to 1:8 Fe^{3+} : (Cys + His) concentration. [2Fe-2S] clusters were synthesized by the addition of $FeCl_3$ (0.33 M stock) and Na_2S (0.33 M stock) to 1:1:16 Fe^{3+}: S^{2-} : (Cys + His) concentration.

UV-Vis absorption and Circular Dichroism spectroscopy: The UV-vis spectra of the samples were recorded inside a glovebox with a Genesys 150 UV-Vis spectrophotometer (ThermoFisher) with an integration time of 0.5 s and an interval of 1 nm. Circular Dichroism (CD) spectra were collected with a JASCO J-815 CD spectrometer, using a scan rate of 200 nm/min (spectral window 200–600 nm). 20 scans were collected. Spectra manager II (JASCO) software was used to analyze data.

Affinity measurements: The peptide solutions were prepared by dissolving the peptides in 20 mM Gly-Gly, pH 8.8 inside a glovebox to a total concentration of cysteine plus histidine of 2.5 mM. After sequential addition of the chosen metal (Fe^{2+}, Co^{2+}), UV-vis spectra were collected and fit with GraphPad Prism v. 6.00 (GraphPad Software, La Jolla California USA) to the following equation: $y = B_{Max} * x^h / (K_d^h + x^h)$, where B_{Max} was the absorbance reached at saturation and h was the Hill slope. For Zn^{2+}, a competition titration against Co^{2+} was used. The Co^{2+} complex was formed at the K_d prior to titration with Zn^{2+}, and the absorption fit to the revised Cheng-Prusoff equation.[43]

Paramagnetic NMR spectroscopy: Samples were prepared in a glovebox, as described above, and 700 μL placed in 5 mm NMR tubes (Sigma-Aldrich) with 10% D_2O. Spectra were recorded at room temperature using a V NMRS four-channel 600 MHz Varian spectrometer (5000 scans, 0.4 s recycle delay, 0.25 s acquisition time).

Cyclic voltammetry: Experiments were conducted under ambient conditions using an electrochemical workstation CHI660 A (CH Instruments). Samples were prepared inside a glovebox and then transferred into a custom-made electrochemical cell. All solutions were purged with argon for 10 min before analysis to ensure that no O_2 was trapped during the transfer from the glovebox to the cell. A standard three electrode cell composed of a glassy carbon working electrode (BASi, 3 mm diameter), an Ag/AgCl reference electrode (1 M KCl) (calibration curve Figure S28), and a platinum wire counter electrode was used for the electrochemical measurements. A scan rate from 50 mVs to 500 mVs was used. No supporting electrolyte was used to avoid interference with stability of the cluster; however, a small amount of NaCl was present from pH adjustment with NaOH and HCl. The working electrode was cleaned with a 0.05 μm aluminum oxide slurry on a polishing cloth and thoroughly rinsed with MilliQ H_2O (Synergy UV water purification system, Merck, Darmstadt, Germany) before each experiment. The reference electrode was sonicated in MilliQ H_2O for 5 min before each experiment.

Acknowledgements

We thank the Simons Foundation (290358FY18 and 290358FY19) and the Natural Sciences and Engineering Research Council of Canada (NSERC) (RGPIN-2020-04375) for funding and A. Dallapè and S. Scintilla for preliminary experiments.

Conflict of Interest

The authors declare no conflict of interest.

Data Availability Statement

The data that support the findings of this study are openly available in Zenodo at https://doi.org/10.5281/zenodo.6425646, reference number 1.

Keywords: bioinorganic chemistry · iron-sulfur clusters · metallopeptides · prebiotic chemistry · Rieske

[1] D. C. Johnson, D. R. Dean, A. D. Smith, M. K. Johnson, *Annu. Rev. Biochem.* **2005**, *74*, 247–281.
[2] L. Belmonte, S. S. Mansy, *J. Chem. Inf. Model.* **2017**, *57*, 3162–3171.
[3] C. Bonfio, *Dalton Trans.* **2021**, *50*, 801–807.
[4] D. W. Bak, S. J. Elliott, *Curr. Opin. Chem. Biol.* **2014**, *19*, 50–58.
[5] E. N. Brown, R. Friemann, A. Karlsson, J. V. Parales, M. M. J. Couture, L. D. Eltis, S. Ramaswamy, *J. Biol. Inorg. Chem.* **2008**, *13*, 1301–1313.
[6] A. R. Klingen, G. M. Ullmann, *Biochemistry* **2004**, *43*, 12383–12389.
[7] J. A. Zuris, D. A. Halim, A. R. Conlan, E. C. Abresch, R. Nechushtai, M. L. Paddock, P. A. Jennings, *J. Am. Chem. Soc.* **2010**, *132*, 13120–13122.
[8] P. Venkateswara Rao, R. H. Holm, *Chem. Rev.* **2004**, *104*, 527–559.
[9] W. Qi, J. Li, C. Y. Chain, G. A. Pasquevich, A. F. Pasquevich, J. A. Cowan, *J. Am. Chem. Soc.* **2012**, *134*, 10745–10748.
[10] B. R. Gibney, S. E. Mulholland, F. Rabanal, P. L. Dutton, *Proc. Natl. Acad. Sci. USA* **1996**, *93*, 15041–15046.
[11] C. Bonfio, L. Valer, S. Scintilla, S. Shah, D. J. Evans, L. Jin, J. W. Szostak, D. D. Sasselov, J. D. Sutherland, S. S. Mansy, *Nat. Chem.* **2017**, *9*, 1229–1234.
[12] J. A. Fee, K. L. Findling, T. Yoshida, R. Hille, G. E. Tarr, D. O. Hearshen, W. R. Dunham, E. P. Day, T. A. Kent, E. Münck, *J. Biol. Chem.* **1984**, *259*, 124–133.
[13] B. Xia, H. Cheng, V. Bandarian, G. H. Reed, J. L. Markley, *Biochemistry* **1996**, *35*, 9488–9495.
[14] J. Lin, T. Zhou, K. Ye, J. Wang, *Proc. Natl. Acad. Sci. USA* **2007**, *104*, 14640–14645.
[15] T. Merbitz-Zahradnik, K. Zwicker, J. H. Nett, T. A. Link, B. L. Trumpower, *Biochemistry* **2003**, *42*, 13637–13645.
[16] M. Lukács, D. Csilla Pálinkás, G. Szunyog, K. Várnagy, *ChemistryOpen* **2021**, *10*, 451–463.
[17] C. D. Douglas, A. V. Dias, D. B. Zamble, *Dalton Trans.* **2012**, *41*, 7782–7791.
[18] D. Rossetto, S. S. Mansy, *Front. Cell Dev. Biol.* **2022**, *10*, 2020–2023.
[19] J. Xu, D. J. Ritson, S. Ranjan, Z. R. Todd, D. D. Sasselov, J. D. Sutherland, *Chem. Commun.* **2018**, *54*, 5566–5569.
[20] M. A. Keller, A. V. Turchyn, M. Ralser, *Mol. Syst. Biol.* **2014**, *10*, 1–12.
[21] K. B. Muchowska, S. J. Varma, J. Moran, *Nature* **2019**, *569*, 104–107.
[22] C. Bonfio, E. Godino, M. Corsini, F. Fabrizi de Biani, G. Guella, S. S. Mansy, *Nat. Catal.* **2018**, *1*, 616–623.
[23] V. Alva, J. Söding, A. N. Lupas, *eLife* **2015**, *4*, 1–19.
[24] V. Sivo, G. D'abrosca, L. Russo, R. Iacovino, P. V. Pedone, R. Fattorusso, C. Isernia, G. Malgieri, *Bioinorg. Chem. Appl.* **2017**, *2017*, 1527247.
[25] S. Scintilla, C. Bonfio, L. Belmonte, M. Forlin, D. Rossetto, J. Li, J. A. Cowan, A. Galliani, F. Arnesano, M. Assfalg, S. S. Mansy, *Chem. Commun.* **2016**, *52*, 13456–13459.
[26] Y. S. Tan, D. P. Lane, C. S. Verma, *Drug Discovery Today* **2016**, *21*, 1642–1653.
[27] L. M. Hunsicker-Wang, A. Heine, Y. Chen, E. P. Luna, T. Todaro, Y. M. Zhang, P. A. Williams, D. E. McRee, J. Hirst, C. D. Stout, J. A. Fee, *Biochemistry* **2003**, *42*, 7303–7317.
[28] L. Valer, D. Rossetto, S. Scintilla, Y. J. Hu, A. Tomar, S. Nader, I. O. Betinol, S. Mansy, *Can. J. Chem.* **2022**, https://doi.org/10.1139/cjc-2021–0237.
[29] V. M. Coghlan, L. E. Vickery, *Proc. Natl. Acad. Sci. USA* **1989**, *86*, 835–839.
[30] R. C. Holz, F. J. Small, S. A. Ensign, *Biochemistry* **1997**, *36*, 14690–14696.
[31] Y. Sugiura, K. Ishizu, T. Kimura, *Biochem. Biophys. Res. Commun.* **1974**, *60*, 334–340.

© 2022 The Authors. ChemBioChem published by Wiley-VCH GmbH

[32] T. A. Link, in *Adv. Inorg. Chem.* **1999**, pp. 83–157.
[33] T. A. Link, W. R. Hagen, A. J. Pierik, C. Assmann, G. von Jagow, *Eur. J. Biochem.* **1992**, *208*, 685–691.
[34] Y. Bromberg, A. A. Aptekmann, Y. Mahlich, L. Cook, S. Senn, M. Miller, V. Nanda, D. U. Ferreiro, P. G. Falkowski, *Sci. Adv.* **2022**, *8*, 1–14.
[35] S. Dagar, S. Sarkar, S. Rajamani, *ChemBioChem* **2022**, *23*, e202200013.
[36] S. Nader, L. Sebastianelli, S. S. Mansy, *Philos. Trans. R. Soc. London Ser. A* **2022**, https://doi.org/10.1098/rsta.2020.0423.
[37] C. Shen, T. Mills, J. Oró, *J. Mol. Evol.* **1990**, *31*, 175–179.
[38] C. Shen, L. Yang, S. L. Miller, J. Oro, *Orig. Life* **1987**, *17*, 295–305.
[39] J. L. Bada, J. H. Chalmers, H. J. Cleaves, *Phys. Chem. Chem. Phys.* **2016**, *18*, 20085–20090.
[40] E. T. Parker, H. J. Cleaves, M. P. Callahan, J. P. Dworkin, D. P. Glavin, A. Lazcano, J. L. Bada, *Origins Life Evol. Biospheres* **2011**, *41*, 201–212.
[41] E. T. Parker, H. J. Cleaves, J. P. Dworkin, D. P. Glavin, M. Callahan, A. Aubrey, A. Lazcano, J. L. Bada, *Proc. Natl. Acad. Sci. USA* **2011**, *108*, 5526–5531.
[42] C. S. Foden, S. Islam, C. Fernández-García, L. Maugeri, T. D. Sheppard, M. W. Powner, *Science* **2020**, *370*, 865–869.
[43] H. C. Cheng, *J. Pharmacol. Toxicol. Methods* **2001**, *46*, 61–71.

Manuscript received: April 8, 2022
Revised manuscript received: June 8, 2022
Accepted manuscript online: June 8, 2022
Version of record online: June 23, 2022

© 2022 The Authors. ChemBioChem published by Wiley-VCH GmbH